Production Engineering (2023) 17:65–79
https://doi.org/10.1007/s11740-022-01151-w

PRODUCTION PROCESS

Joining of multi-material structures using a versatile self-piercing riveting process

Fabian Kappe[1] · Simon Wituschek[2] · Mathias Bobbert[1] · Michael Lechner[2] · Gerson Meschut[1]

Received: 19 April 2022 / Accepted: 19 July 2022 / Published online: 5 August 2022

Abstract
Due to the increasing use of multi-material constructions and the resulting material incompatibilities, mechanical joining technologies are gaining in importance. The reasons for this are the variety of joining possibilities as well as high load-bearing capacities. However, the currently rigid tooling systems cannot react to changing boundary conditions, such as changed sheet thicknesses or strength. For this reason, a large number of specialised joining processes have been developed to expand the range of applications. Using a versatile self-piercing riveting process, multi-material structures are joined in this paper. In this process, a modified tool actuator technology is combined with multi-range capable auxiliary joining parts. The multi-range capability of the rivets is achieved by forming the rivet head onto the respective thickness of the joining part combination without creating a tooling set-up effort. The joints are investigated both experimentally on the basis of joint formation and load-bearing capacity tests as well as by means of numerical simulation. It turned out that all the joints examined could be manufactured according to the defined standards. The load-bearing capacities of the joints are comparable to those of conventionally joined joints. In some cases the joint fails prematurely, which is why lower energy absorptions are obtained. However, the maximum forces achieved are higher than those of conventional joints. Especially in the case of high-strength materials arranged on the die side, the interlock formation is low. In addition, the use of die-sided sheets requires a large deformation of the rivet head protrusion, which leads to an increase in stress and, as a result, to damage if the rivet head. However, a negative influence on the joint load-bearing capacity could be excluded.

Keywords Mechanical joining · Self-piercing riveting · Multi-material design · Joining technology · Versatile process

1 Introduction

The limitation of natural resources and far-reaching changes in climate policy to reduce CO_2 lead to the application of different strategies in order to achieve the climate targets. Here, the strategy is to pursue both the development of new drive concepts and the use of lightweight designs in car body [1]. In particular, the use of multi-material design allows weight to be saved by adapting the structure to the application of load. However, conventional thermal joining technologies are reaching their limits due to the use of combining different materials and metallurgical incompatibilities with a focus on process robustness. Therefore, for these joining tasks, mechanical joining methods are increasingly being used. The increasing number of multi-material joints as well as lightweight structures, has led to the development of a variety of mechanical joining technologies. Due to its high load-bearing capacities, a wide range of application and high process robustness, semi-tubular self-piercing riveting

✉ Fabian Kappe
fabian.kappe@lwf.upb.de

Simon Wituschek
simon.wituschek@fau.de

Mathias Bobbert
mathias.bobbert@lwf.upb.de

Michael Lechner
Michael.Lechner@fau.de

Gerson Meschut
meschut@lwf.upb.de

[1] Laboratory for Material and Joining Technology (LWF®), Paderborn University, Paderborn, Germany

[2] Institute of Manufacturing Technology (LFT), Friedrich Alexander University Erlangen Nuremberg, Erlangen, Germany

mentioned in DIN 8593–5, 2003 [2], which is also one of the mechanical joining processes, is being frequently used. Voelkner et al. (1996) showed, that the self-piercing riveting (SPR) process can be divided into four stages (Fig. 1) [3]. First, the blank holder, which encloses the rivet, fixes the sheets on the die. Subsequently, the punch presses the rivet into the punch-sided sheet, initiating a cutting phase. The rivet penetrates the punch-sided sheet and the resulting slug is stored in the shank of the rivet. If the feed rate is further increased, the rivet undergoes plastic deformation and expands radially into the die-sided sheet, resulting in the formation of an interlock. By upsetting the rivet, a force-fit and form-fit connection is created. Finally, the punch and the blank holder reset to their initial position.

The development of conventional semi-tubular rivets was based on aluminium-aluminium joints as well as (high-strength) steel-aluminium joints. Nevertheless, these elements reach their application limits if higher strength materials such as press hardened steels are to be joined. However, the increasing number of material-thickness combinations, the rising number of materials used and the currently rigidly designed tool systems, result in the need for a large number of rivet-die combinations [5]. In addition, the currently rigid joining systems require a tool adjustment when major changes according to the boundary conditions such as material thickness, the formability of the sheets or the arrangement of the parts to be joined occur, in order to ensure the required characteristics of the joint.

Figure 2 illustrates some of the possibilities for adapting the semi-tubular riveting process to changing boundary conditions. One possible research approach in order to extend the application limits of the SPR technology is the development of new rivet geometries that enable multi-range capability or the joining of different material combinations and thus increase the range of application. In addition to changing the auxiliary joining parts, changing the process kinematics can also extend the process limits and enable an increase in flexibility and versatility. Below, some of the listed methods are presented in detail in order to classify the V-SPR process accordingly in the state of the art.

The development of Trinick (2015) was aimed to design a new rivet geometry to create multilayer connections which, in particular, present challenges for rigid tool systems as the limited rivet cavity and the partly absorbed punching slug result in an undefined joint formation. This rivet geometry eliminates the limitation of the shank volume using a hollow design, which enables process-reliable multi-layer connections to be produced. In addition, the hollow design of the rivet allows a certain multi-range capability [6].

The investigation by Uhe et al. (2020) also focused on increasing flexibility by developing a stress-optimised rivet geometry. It enables the joining of a combination of aluminium and high-strength steel as well as a connection of pure high strength steels with a single rivet geometry, for which otherwise different rivet geometries would be required. To create a greater cavity for the slug, the inner rivet diameter

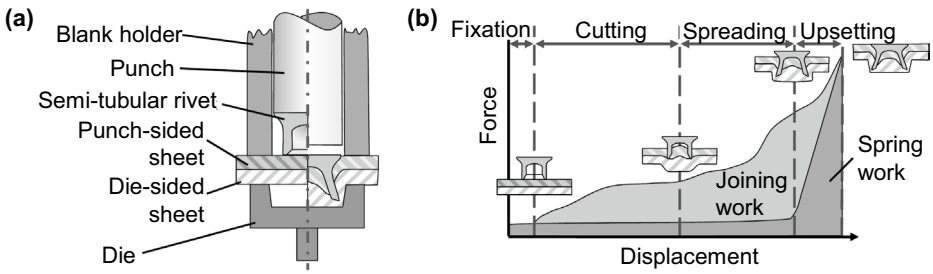

Fig. 1 Tooling for SPR (**a**) and process sequence of the SPR process before (left) and after (right) joining as well as the exemplary joining force–displacement curve (**b**) according to [4]

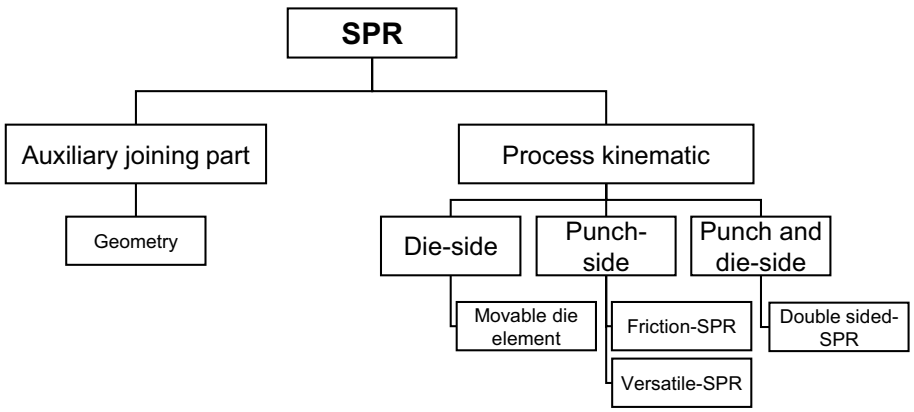

Fig. 2 Exemplary possibilities of influencing the SPR process to increase the process range as well as the flexibility and versatility

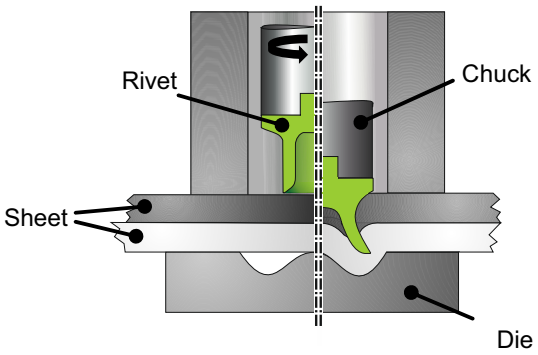

Fig. 3 Process sequence of the FSPR process before (left) and after (right) joining [8]

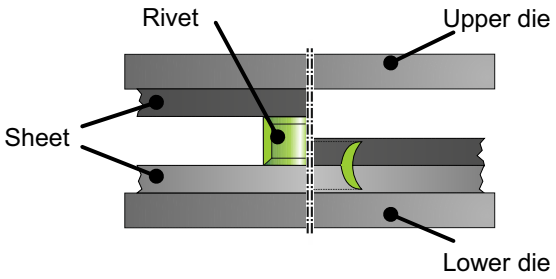

Fig. 4 Process sequence of the DSSPR process before (left) and after (right) joining [9]

was extended and the outer shank was bevelled to reduce stress- and strain peaks [7].

A modification of the system kinematics can also increase the versatility of the joining process, as tool changes can be reduced or joining processes can be adapted to a new joining task by the changed kinematic. Li et al. (2013) presented a friction self-piercing riveting (F-SPR) process, which offers the possibility of extending the application limits, especially for brittle materials, by using completely new process kinematics. Here, the rivet is rotated at high speed during the joining process, resulting in plastification of the punch-sided joining part (Fig. 3). The formation of cracks can thus be prevented. Through the plastification of the parts to be joined, the process combines the solid-state joining mechanisms of friction stir spot welding and the mechanical joining mechanism of semi-tubular self-piercing riveting [8].

Alves et al. (2020) developed a double-sided self-piercing riveting (DS-SPR) for the formation of a planar joint by mechanical joining processes when using multi-material structures (Fig. 4). In this joining process, a tubular joining part is inserted between two joining parts. Subsequently, these are pressed together under high pressure. The auxiliary joining part penetrates both the upper and the lower sheet and forms an interlock in both parts to be joined. The result is a non-detachable, flat and two-sided impermeable joint. Advantages of this process are, for example, the independence of the sheet thickness as well as the low-cost production of the auxiliary joining parts [9].

Neugebauer et al. (2010) increased process efficiency in self-piercing riveting with a solid rivet by means of improved die-side tool actuation. Hereby, the joining force could be reduced by up to 30%. In addition, an increased joint load-bearing capacity could be achieved [10].

Kappe et al., (2022a) presented a versatile self-piercing riveting (V-SPR) process which combined new multi-range capable rivets and a joining system with extended punch-sided tool acutator technology [11]. The first multi-range capable rivet (without head deformation) consists of a tubular rivet with ring grooves in the rivet head area. During joint formation, the punch-sided sheet is formed into theses ring grooves creating an interlock between the sheet and the rivet head. Using the second multi-range capable rivet, the joint is created by deforming the rivet head. The process sequence required for the V-SPR joining process, is shown in Fig. 5 for the rivet with head deformation. For this purpose, a system with an inner and an outer punch as well as a blank holder is required. The closing head is formed by a die. Basically,

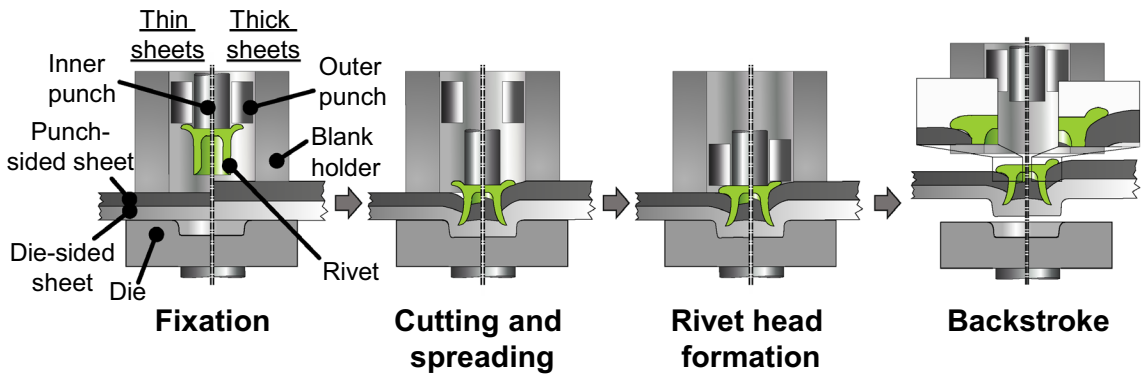

Fig. 5 Process sequence for V-SPR with head deformation [11]

the process sequence can be divided into four process stages. First, the sheets are placed between the punches and the die, and they are fixed by the blank holder. Subsequently, the setting process is initiated by the inner punch. In this stage of the process, the rivet first punches through the punch-sided sheet metal and forms an interlock in the die-sided joining part by plastic deformation. After setting, a forming process is carried out by the outer punch. The inner punch remains in the setting position and stabilises the rivet. In joint formation using the multi-range capable rivet with head deformation, the protrusion of the rivet head is formed onto the punch-sided joining part by the outer punch. The subsequent forming takes place according to the respective thickness of the joint, allowing the process to react adaptively to changing boundary conditions. Finally, the inner and outer punch as well as the blank holder reset to their initial position and the joint can be removed from the die.

Kappe et al., (2022a) examined three different pure aluminium joints using both rivet concepts. The increased punch-sided tool kinematic combined with the use of multi-range capable rivets enabled the process to be adapted to the respective thickness of the joint without changing the tooling or rivets. Changes of the sheet thickness of up to 1.0 mm could be covered. Especially the number and degree of filling of the ring grooves significantly influenced the load bearing capacity of the rivet without head deformation. Under cross tensile load, only low strength of 600 N for a combination of EN AW-6014 1.0 mm and EN AW-6014 2.0 mm could be achieved. High load-bearing capacities under shear and cross tensile load between 2 and 4 kN could be reached using the rivet with head deformation. These are comparable to the behaviour of conventionally SPR joints [11].

Since the previous results of research conducted on the V-SPR process are based on pure aluminium joints, the process principle is applied to multi-material joints in this study. These represent a major application, especially in the mobility sector. The process is analysed using experimental investigations as well as numerical simulation in order to identify cause-effect-relationships.

2 Experimental procedure

2.1 Materials

In this study, different typical automotive material-thickness combinations and materials are used. All joints are designed as multi-material joints. As aluminium material, the wrought aluminium alloy EN AW-6014 T4 with sheet thickness 1.0 mm, 1.5 mm and 2.0 mm is used. The aluminium sheet is combined with the dual phase steel HCT590X in sheet thicknesses 0.8 mm, 1.0 mm and 1.5 mm. The newly developed rivets were made of a C35 steel, tempered to a hardness of 480 HV and ALMAC coated. The material C35 is well-suited for the development of the new rivets, as it has good ductility and strength properties even in the hardened state. The chemical composition and the mechanical properties of the sheet materials used are shown in Table 1.

2.2 Joining and test set-up

In order to investigate the capability of the multi-range capable rivets on joining multi-material designed joints, the rivet with head deformation is joined using a specially developed joining system with extended punch-sided tool actuator technology. which was presented by [11]. The servo-electric drives of the inner and the outer punch, which are controlled by displacement, enable joining forces of up to 80 kN and setting speeds of up to 80 mm/s. Joining speed of 5 mm/s was defined for all specimens joined for this investigation. The movements of the punches can be defined completely independently. A Tox TE-X joining system is used to produce conventional SPR-joints, which are used to compare and evaluate the load-bearing capacities of the multi-range capable rivets. Also in this system, the punch feed is realised using an servo-electric drive, which is controlled by force. Maximum joining forces of up to 80 kN and maximum joining speeds of 200 mm/s can be achieved. In this investigation, all conventionally joined specimens were joined at a speed of 20 mm/s. The characteristics of both two joining systems used are shown in Fig. 6.

The created joints are evaluated according to the joint formation and the joints load-bearing capacity. For the SPR process, various quality-relevant characteristics are defined to evaluate the quality of a joint. In this study, the most important parameters interlock, minimum die-side material thickness and rivet head position are considered (Fig. 7, left). For the evaluation of the quality of the V-SPR joints.

Kappe et al. [11] extended theses quality-relevant characteristics to include the protrusion height and the gap height (Fig. 7, right). In both joints, the closing head diameter is determined in order to measure the cavity filling of the die.

For the load-bearing capacity, shear tensile and cross tensile tests according to the DVS/EFB-Merkblatt 3480–1 are carried out [15]. For all tests, the universal testing machine manufactured by Zwick (Fig. 8, left) was used. This testing machine enables a force range of up to 100 kN to be tested. All tests are carried out quasi-statically at a test speed of 10 mm/min and the force and displacement values are determined during the test to record the test data. For the cross tensile tests, the machine measurement system is used for logging the test data of the displacement. When testing the shear tensile test specimens, an additional local displacement measuring system using a sensor arm extensometer is used. The used test specimens are shown in Fig. 8, right. For the shear tensile test, two

Table 1 Chemical composition of the used aluminium alloy EN AW-6014 T4 [12] and the dual phase steel HCT590X [13] and mechanical properties of both materials [14]

EN AW-6014 T4									
Chemical composition (weight %)									
Elements	Si	Fe	Cu	Mn	Mg	Cr	Zn	Ti	V
Min.	0.30			0.05	0.40				
Max.	0.60	0.35	0.25	0.20	0.80	0.20	0.10	0.10	0.10

HCT590X								
Chemical composition (weight %)								
Elements	C	Si	Mn	P	S	Al	Cr+Mo	Nb+Ti
Min.						0.015		
Max.	0.15	0.75	2.50	0.04	0.015	0.15	1.40	0.15

Mechanical properties

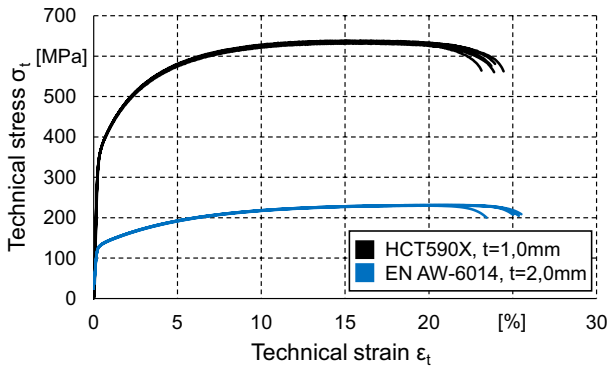

Test method
Quasistatic tensile test
Strain rate
0.01 1/s
Deformation measurement
GOM Aramis
Specimen geometry
According to DIN 50125

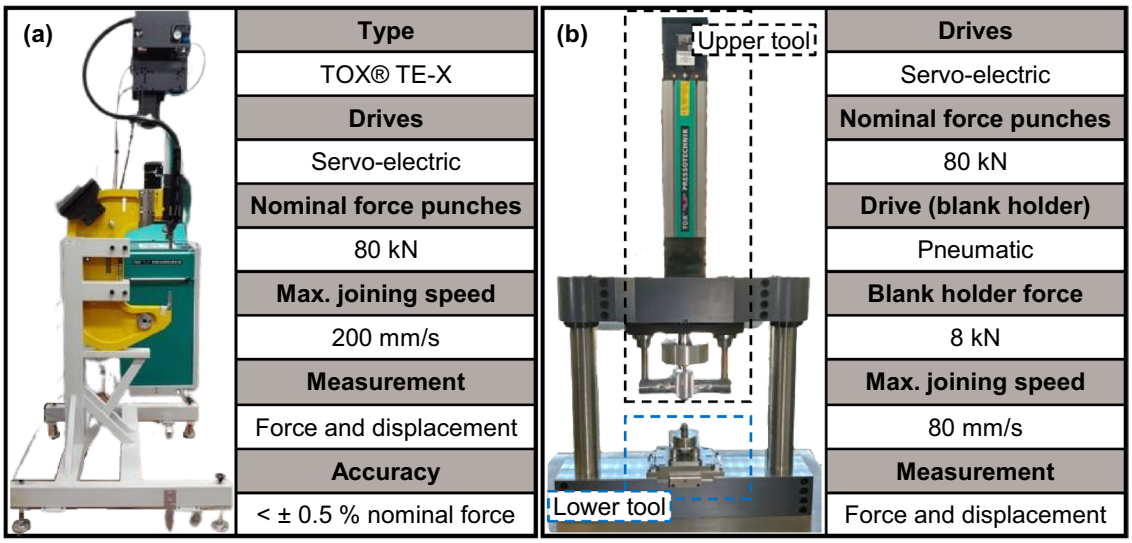

Fig. 6 Joining systems used; left: TOX-TE-X to process the conventional self-piercing rivets (**a**), right: Joining system with extended punch-sided tool actuator technology to process the versatile self-piercing rivets (b) [11]

sheets with dimensions 45 mm × 105 mm are joined with an overlap 16 mm. The joint is located in the geometric centre of the overlap. The specimens are tested to failure and evaluated according to the failure pattern as well as the curve characteristics. For the cross tensile test, two crosswise overlapped blanks with dimensions 50 mm × 150 mm are jointed with the joint placed in the geometric centre of the joint. Again, the specimens are tested to failure and evaluated analogously to the procedure described above.

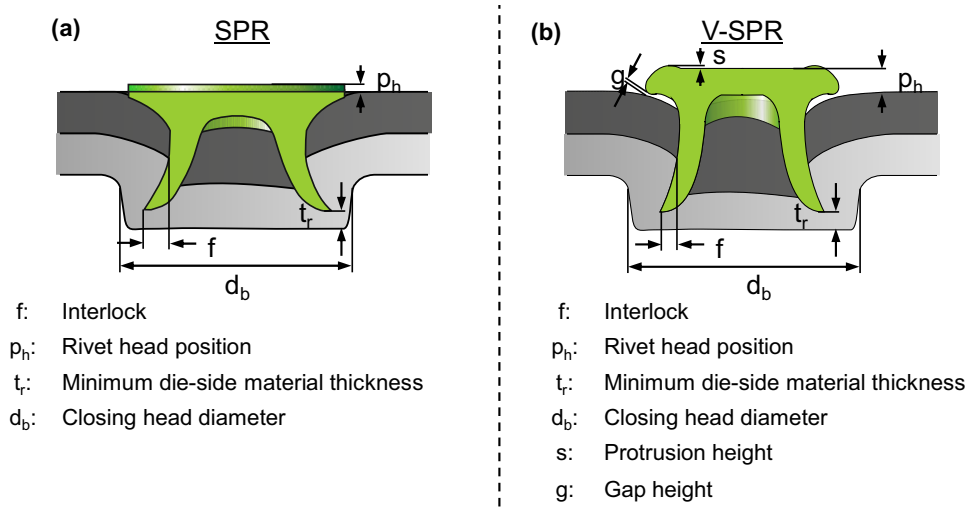

Fig. 7 Quality relevant parameters used to evaluate the joint formation; left: SPR (**a**), right: V-SPR according to [11] (**b**)

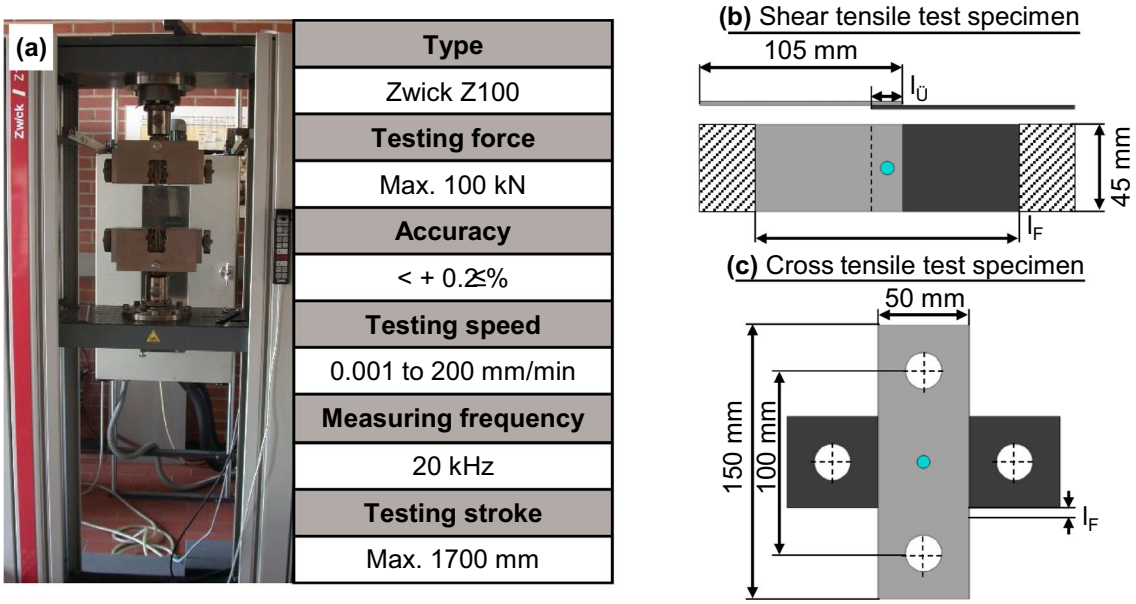

Fig. 8 Test set-up used to determine the load-bearing capacity; left: Universal testing machine Zwick Z100 including technical data (**a**), right: Schematic illustration of the specimen geometries: shear tensile test specimen (**b**) and cross tensile test specimen (**c**)

2.3 Simulative process design

In an initial substitute model, which focused only on the rivet head geometry, it was possible to demonstrate the feasibility of the two rivet concepts presented above [16]. In this investigation, the entire joining process of the V-SPR process is now considered, which takes account of both the setting and the forming of the rivet head and thus enables the numerical analysis of the V-SPR process.

For this purpose, a 2D axisymmetric simulation model is built and implicitly calculated in the LS-Dyna simulation software (Fig. 9). For the calculation, the solver smp_d_R910 was used. The model consists of an inner and an outer punch, a blank holder, the rivet, the parts to be joined and the die. Both punches as well as the die are modelled as elastic components. The blank holder was designed as a rigid body. In the lower area of the die, the force of the joining process is measured using a cross-section. Static coefficients of friction were used to describe the contact behaviour between the different parts. The constant values represent an average value and thus a simplification of the complex friction condition during the joining process. However, it has already been proven that this simplification leads to a good agreement between simulation and experiment.

The joining process is controlled by the displacement of the inner and the outer punch. The movements of the

FE-simulation – Relevant parameters	
Simulation software	LS-Dyna
Solver	smp_d_R910
Analysis	Implicit
Section	Shell
Element formulation	Axissymmertric solid
Elements Start	approx. 4000
Elements End	approx. 22000
Material seperation	Geometrical
Process control	Displacement
Contact setting	Constant static friction coefficient
Average CPU time	15 minutes

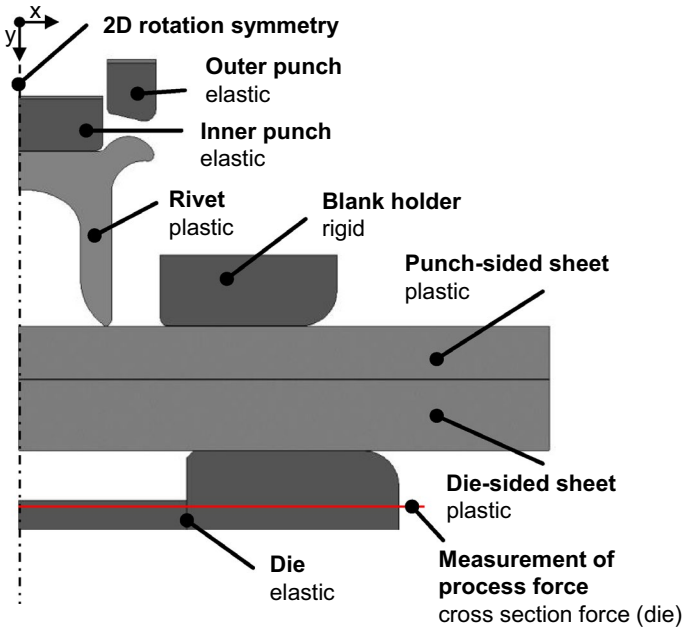

Fig. 9 Numerical setup of the new joining process considering setting and forming process

punches are adapted to the material flow of the parts to be joined, the design of the joint in terms of minimum die-side material thickness and interlock as well as the formation of the rivet head. The joining process is simulated including the relief process to be able to evaluate the joining properties without any load.

Particularly decisive for the calculation of the joining process is the remeshing of the deformed parts. Especially in the areas of large deformations, local element penetrations or distortions of the elements, a remeshing algorithm is used. In the model set up here, complete remeshing of the joining parts as well as the rivet takes place in previously defined time steps with a predefined element length of 0.05 mm.

In order to represent the flow behaviour of the materials in the simulation, the flow curves were implemented. These were determined by compression test according to DIN 50106 and subsequently extrapolated using the Hocket-Sherby approach for the sheets [14] and rivet material [16].

3 Results and discussion

3.1 Process analysis

In order to analyse the applicability of the V-SPR process on multi-material combinations, three different typical automotive material-thickness combinations were chosen for this investigation (Table 2). Two material-thickness combinations were chosen in order to fulfil the preferred joining directions for semi-tubular self-piercing riveting of hard to soft and thin to thick. The third combination does not meet these two criteria. For these selected material thickness combinations, the multi-range capability of the rivets should also be analysed, which is why different total package thicknesses were selected. The selected material combinations do not represent the process limits of the new joining process at present, rather they form the basis for the initial transferability studies to multi-material structures.

Table 2 Material-thickness combinations used to analyse the applicability of the V-SPR process on multi-material combinations

Nr	Punch-sided sheet	t [mm]	Die-sided sheet	t [mm]
1	HCT590X	0.8	EN AW-6014, T4	2.0
2	HCT590X	1.0	EN AW-6014, T4	1.5
3	EN AW-6014	1.5	HCT590X	1.5

To create all joints, a die with a diameter of 9.5 mm was used. For combination 1 a die depth with 1.4 mm was chosen. Due to the lower die-sided material thickness, Combination 2 and Combination 3 were joined using a die depth of 1.2 mm.

For all three sheet thickness combinations, the quality-relevant parameters shown above can be evaluated and a suitable joint can be achieved in all combinations. The minimum die-side material thickness and the interlock are within acceptable ranges (Fig. 10).

Since the interlock is decisive for the joint load-bearing capacity, this geometric parameter is evaluated initially. A pronounced interlock is achieved in particular within the

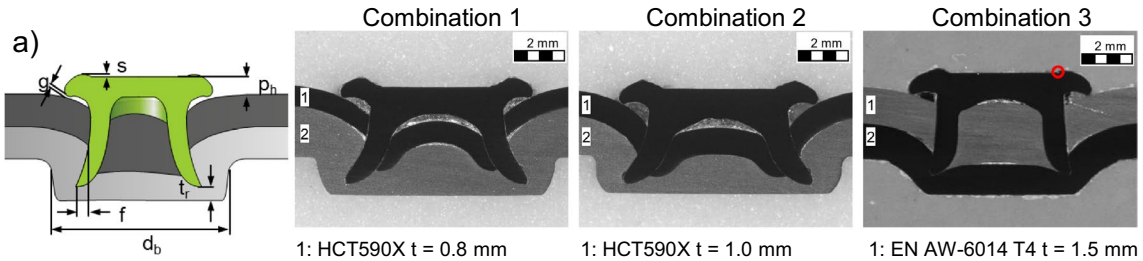

Joint characteristic	Combination 1	Combination 2	Combination 3
f:	0.79	0.61	0.12
p_h:	-0.09	0.08	0.54
t_r:	0.53	0.42	0.76
d_b:	9.50	9.48	9.54
s:	0.36	0.33	0.14
g:	0.02	0.00	0.04

Average values, number of specimens tested: 3

Fig. 10 Analysis of the joint formation using defined quality-relevant parameters (**a**) by means of macrosections (left: HCT590X t = 0.8 mm in EN AW-6014 T4 t = 2.0 mm [Combination 1]; centre: HCT590X t = 1.0 mm in EN AW-6014 T4 t = 1.5 mm [Combination 2]; right: EN AW-6014 T4 t = 1.5 mm in HCT590X t = 1.5 mm [Combination 3])

joints that fulfil the preferred joining direction. In particular, the steel slug is responsible for this. After cutting through the punch-sided sheet metal, the slug supports the expansion of the rivet. This effect is much more significant with steel materials than with softer materials such as aluminium, as Combination 3 shows. The spreading of the rivet is additionally supported by the deep penetration of the rivet into the sheets, which is shown by the low rivet head position in combination 1 and 2. In addition, a slight forming of the rivet head protrusion from about 0.1 mm is sufficient to close the joint which is shown by the measured protrusion height after forming (initial rivet head protrusion height 0.4 mm).

In combination 3, the rivet does not penetrate deep into the joint due to the high material strength of the punch-sided joint part. Increasing the penetration could lead to the collapse of the shaft as a consequence of the increasing stresses. Due to the low penetration depth, there is hardly any spreading of the rivet. Only a very small interlock is achieved at the defined minimum value.

Due to the high standing of the rivet in combination 3 after the joining process, a large forming is required to close the joint and minimise the gap height. The protrusion height s after the forming process is merely 0.14 mm. The large degrees of deformation leads to an increased risk of cracking in the head area. In this joint, the transition area from the joining surface and the rivet head protrusion already shows first superficial cracks (Fig. 10, red marks). These can lead to an impairment of the joint load-bearing capacity and might cause a reduction in corrosion resistance.

The determined gap heights between the protrusion of the rivet head and the punch-sided joint part is in all joints low or not existent. Nevertheless these air inclusions may cause problems in following process steps such as CDP coating. In addition, these hollows might have an influence on the corrosion resistance of the joint, if a corrosive medium penetrates into these cavities. Further investigations are being pursued targeting a change of the head geometry to reduce the cavities while maintaining the multi-range capability as well as the load bearing-capacietes.

For further analysis of the forming process, the process simulation shown above is used. Due to the comparability to conventional semi-tubular self-piercing riveting, the setting process with the cutting of the punch-sided joint part and the spreading of the rivet will not be considered further here. The validation of the simulation model performed by comparing the numerically calculated geometry with the macro section as well as by comparing the quality relevant parameters (Fig. 11). The comparison shows that the joining and forming process is reproduced to a high degree. Furthermore, the deformation behaviour of the rivet and sheet material used is well reproduced. The feed-in behaviour of the sheets into the die and around the rivet foot as well as the flow and rising behaviour of the punch-sided sheet into the rivet shank can be accurately reproduced. In addition, the quality relevant parameters are reproduced to a considerable level. There are only minor deviations, which are to be considered acceptable. Since the simulation shows extensive agreement it is regarded as validated and will be used for further investigations.

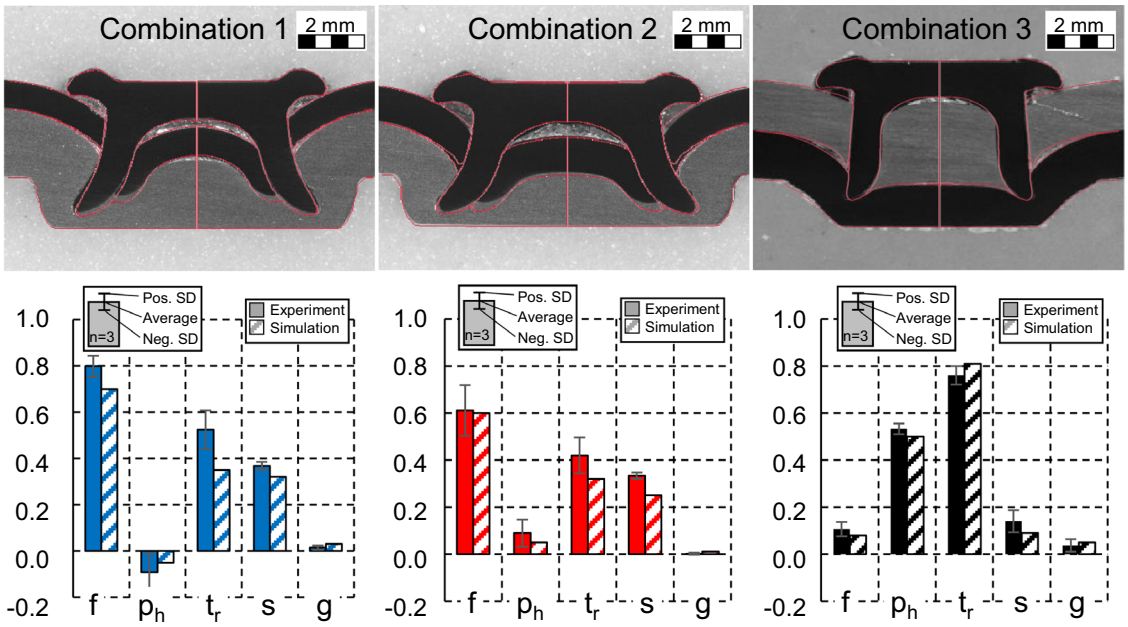

Fig. 11 Validation of the V-SPR process simulation by means of joint formation and quality-relevant parameters (left: HCT590X t = 0.8 mm in EN AW-6014 T4 t = 2.0 mm [Combination 1]; centre: HCT590X t = 1.0 mm in EN AW-6014 T4 t = 1.5 mm [Combination 2]; right: EN AW-6014 T4 t = 1.5 mm in HCT590X t = 1.5 mm [Combination 3])

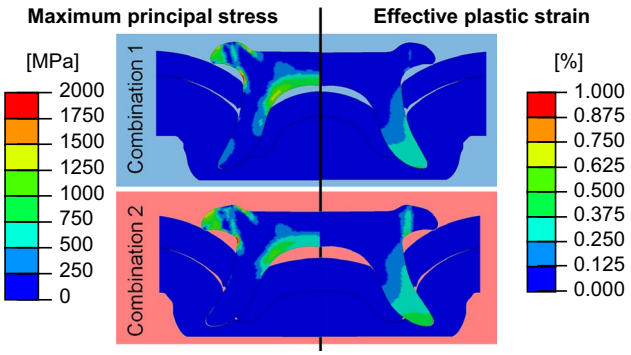

Fig. 12 Internal maximum principal stress (left) and effective plastic strain (right) distribution after joining process (top: HCT590X t = 0.8 mm in EN AW-6014 T4 t = 2.0 mm [Combination 1]; bottom: HCT590X t = 1.0 mm in EN AW-6014 T4 t = 1.5 mm [Combination 2])

Figure 12 shows the distribution of the internal maximum principal stress on the left and the effective plastic strain on the right side for the combination 1 and 2. Both macrosections could show that there is no cracking in the rivet. The greatest stress concentration in both joints occurs in the rivet head protrusion due to the forming process. However, the increased forming in combination 2 does not lead to a significant increase in tensile stresses. In particular, the deeper penetration of the rivet ensures that deep forming and an increase in stress concentration can be avoided.

The supporting effect of the steel slug is shown in both joints by the tensile stresses in the inner area of the rivet shaft. In combination 1, the slug rises higher into the shaft, resulting in greater expansion of the rivet. However this also results in a concentration of tensile stress. Excessive tensile stresses could lead to cracking in this area, which is why they should be avoided. However, the numerical data do not indicate a need for modification of the geometry in this case.

In both joints, the maximum stress concentration is located in the transition area between the joining surface and the rivet head as well as the rivet head and the rivet shank. The greatest plastic deformation occurs during the spreading of the rivet in the rivet shank respectively rivet foot. However, the reduction of the protrusion height (s) by 0.04 mm leads to a rather large change in the distribution of the effective plastic strain in the head area.

The greatest strain is concentrated at the transition between the rivet head and the rivet shank and decreases with increasing distance in the direction of the rivet head. The strain occurs in a narrow band so that no deformation appears in the outer area. The concentrated forming in this area, may cause damage to the rivet material, which could lead to premature failure of the joint.

After relieving the joint, high stress concentrations can be found, especially in the transition area between the rivet shank and the rivet head protrusion. These are caused by springback effects of the rivet material as well as the punch-sided joining part. A negative effect on the quasi-static load-bearing capacity is not to be expected. However,

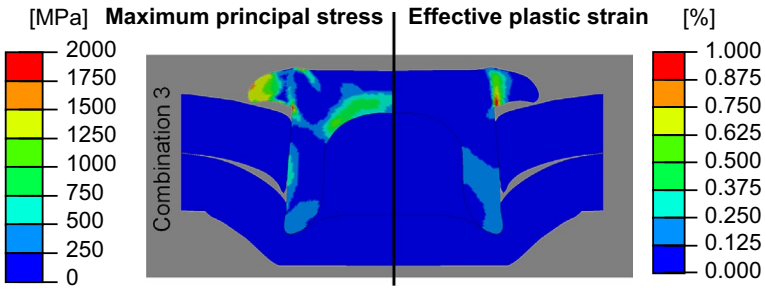

Fig. 13 Numerical analysis of the internal stress states during different stages of the joining process (left: Rivet completely set; centre: intermediate step during forming process; right: Rivet head formed and joint relieved from the punches stress)

these stresses might lead to crack initiation, especially under cyclic load. Further investigations are intended to examine this issue and, if necessary, modify the rivet geometry with this regard.

The numerical investigation of combination 3 shows a significantly different stress and strain distribution. Due to the lower penetration of the rivet into the joint, a greater deformation of the rivet head is required. This is reflected in the higher tensile stresses in the rivet head protrusion and the strong increase in plastic strain. The area with the greatest plastic strain is again arranged in a narrow band between the rivet shank and the rivet head. The high-strength steel material also prevents the rivet from spreading, resulting in low strain at the base of the rivet.

Furthermore, the rivet shaft begins to collapse, as can be seen by the increased stress concentration on the outside of the rivet shaft. An increase in the setting depth by the inner punch would therefore probably not contribute to an improvement of the joint formation. Buckling of the rivet shaft and thus unacceptable joint formation would result. The thickening of the shank could prevent buckling of the rivet. However, the stiffer design of the rivet could also negatively affect the expansion of the rivet an thus interlock and minimum die-side material thickness formation.

As a result of the aluminium material on the punch side, the tension inside the rivet shaft decreases. The supporting spreading effect of the slug is thus reduced.

Due to the buckling of the rivet shaft as well as the crack formation which is visible in the macrosections, the numerical analysis of combination 3 is extended to the different process stages of the setting of the rivet and the forming of the rivet head (Fig. 13). Hereby, correlations between the stress distribution in the rivet and the crack formation in the rivet head shall be further investigated.

Initially, it is shown that the buckling of the shank already occurs during the setting process. The rivet shank upsets during the penetration of the rivet into the die-sided sheet. During the following forming process, no further increase in stress concentration is observed.

During the forming process, the highest stress concentration occurs in the transition between the joining surface of the rivet and the rivet head protrusion. Here maximum stresses of approx. 2300 MPa are reached. As a result, due to the great rivet head deformation first cracks are visible in the macrosections.

Particularly in the case of loads acting on the head, this could be the location of additional crack growth, which could lead to failure of the joint. In addition, the cracks in the head area increase the risk of corrosion failure. The stress accumulation located in the transition area could be reduced in further investigations by increasing the radius in this area to prevent crack initiation and possible premature failure of the joint.

In addition, the forming process also leads to an increased stress concentration in the rivet foot. These stresses are comparatively low, but may cause a deeper setting of the rivet in the case of softer die-sided joining partner used. This may result in a reduction of the minimum die-side material

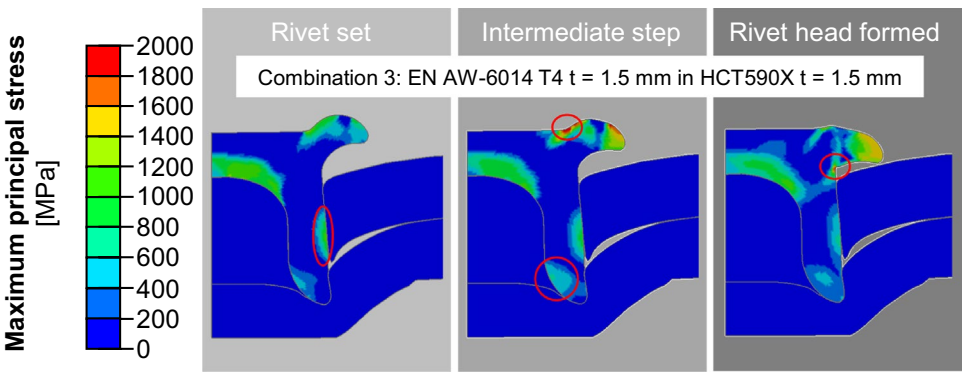

Fig. 14 Internal maximum principal stress (left) and effective plastic strain (right) distribution after joining process (EN AW-6014 T4 t = 1.5 mm in HCT590X t = 1.5 mm [Combination 3])

thickness and should be considered when defining the process parameters.

The third simulation stage indicates that the tensile stresses increase in the transition area between the rivet head and the rivet shank after the joint has been relieved of load. However, as Fig. 14 showed, this is the area where the greatest plastic strain occurs. An increase in stresses can therefore lead to cracking as a result of strain hardening caused by the forming process and the exhausted elongation possibilities of the rivet material.

As cracks were detected in the macrosection of this combination, the numerical analysis is additionally extended to the triaxiality during the forming process (Fig. 15). This allows the results to be embedded within the basic damage criteria to cracking in opening mode I. The analysis shows that negative triaxiality prevails especially in the rivet shaft. This confirms the above-mentioned statement about the supporting spreading effect of the slug. Further pressure areas can be identified in the transition area between the rivet shank and the rivet head protrusion.

Especially in the transition area between the joining surface of the rivet and the rivet head protrusion triaxiality values between 1/3 (uniaxial tension) and 2/3 (biaxial tension) are achieved. This is the area where the crack occurred as well as the highest stress concentration prevails. The analysis of the triaxiality thus supports the above mentioned findings on the occurrence of cracks in the joint as a result of the occurring tensile stresses.

3.2 Investigation of the load-bearing capacity

In order to examine the joints load-bearing capacity shear and cross tensile tests are performed according to the above described procedure. To evaluate these results, the load bearing behaviour is compared with conventionally created joints. These were sampled according to the approach described in [17] with regard to the quality-relevant parameters interlock (f), minimum die-side material thickness (t_r) and rivet head position (p_h) The quality-relevant characteristics are shown in Table 3. To create the conventional SPR-joints, 2 different rivet length and 3 different die geometries were required.

Considering the results of the joint load-bearing capacity under shear tensile load (Fig. 16), it is noticeable that at least comparable, rather greater maximum forces can be achieved for all joints. However, two out of three connections fail prematurely, which is why less energy can be absorbed.

Especially in combination 1, the maximum force and the energy absorbed is significantly increased. In order to be able to evaluate the load-bearing capacity under shear tensile load, the fracture patterns are included into the analysis in addition to the curves characteristics and the data measured.

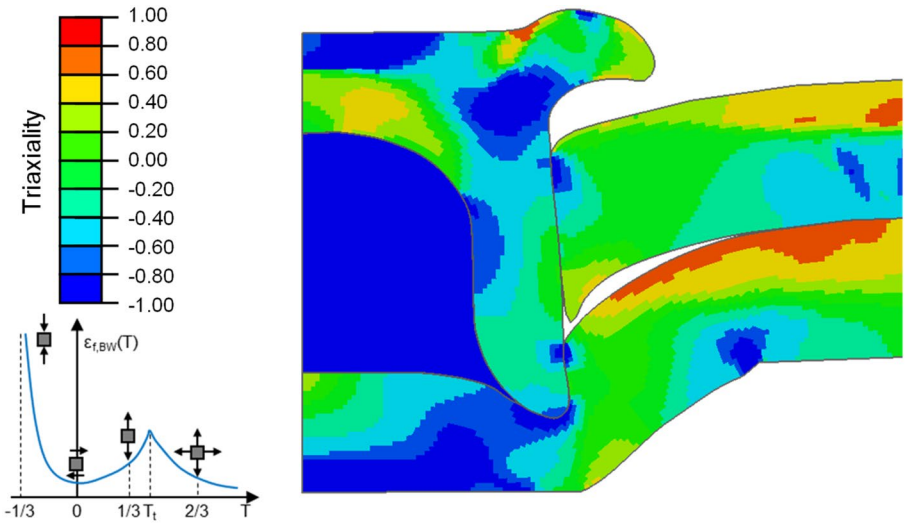

Fig. 15 Numerical analysis of triaxiality during the forming process (EN AW-6014 T4 t = 1.5 mm in HCT590X t = 1.5 mm [Combination 3])

Table 3 Summary of the quality-relevant characteristics for combinations 1 to 3 for conventional SPR (left), and V-SPR (right)

Average values, number of specimens tested: 3	SPR			V-SPR		
	f	t_r	p_h	f	t_r	p_h
Combination 1	0.45	0.52	0.06	0.77	0.43	− 0.12
Combination 2	0.44	0.45	0.03	0.48	0.32	0.00
Combination 3	0.21	0.37	− 0.25	0.12	0.76	0.54

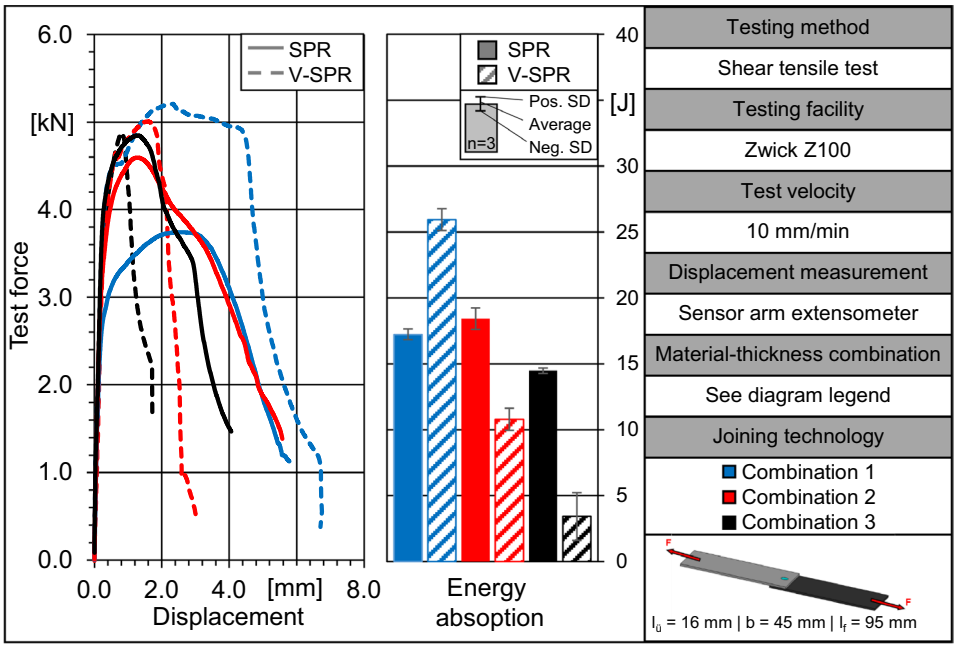

Fig. 16 Load bearing tests under shear tensile load; left: Exemplary test force-displacement curves for the SPR and V-SPR riveted joints for combinations 1–3, right: Comparison of the achieved energy absorption for the SPR and V-SPR riveted joints for combinations 1–3

Exemplary fracture patterns of the three combinations are shown in Fig. 17.

There are two reasons that explain this behaviour. On the one hand, a large interlock is achieved, which is mainly responsible for the load-bearing capacity. This is almost twice as large as the interlock of the SPR-joint. The enlargement is due to the longer shank of the multi-range capable rivet compared to the 4.5 mm long rivet used in conventional joining. Despite the increased rivet length, the steel slug supports the rivet to spread which is why the minimum die-side material thickness is not reduced considerably. On the other hand, the rivet head, which is formed onto the punch-sided sheet after the setting process, supports the strong energy absorption. In both joints (SPR and V-SPR), the joint fails due to the fracture of the thin steel joining partner on the punch side. In conventional processes, the part to be joined subsequently unbuttons from the head area of the rivet. In the V-SPR process, in addition to the failure of the joining part, the rivet is also pulled out of the joint, as the head is formed onto the punch-sided sheet. This results in a later

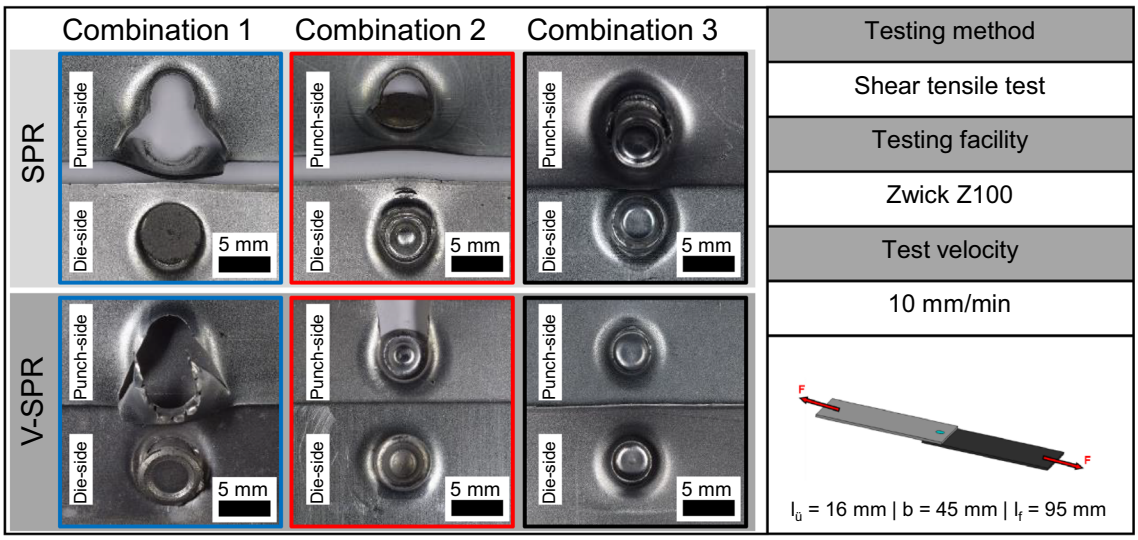

Fig. 17 Compilation of exemplary fracture patterns under cross tensile load for combination 1–3 (left: HCT590X t = 0.8 mm in EN AW-6014 T4 t = 2.0 mm [Combination 1]; centre: HCT590X t = 1.0 mm in EN AW-6014 T4 t = 1.5 mm [Combination 2]; right: EN AW-6014 T4 t = 1.5 mm in HCT590X t = 1.5 mm [Combination 3])

drop in force and the constant holding of the force at a similar level of the maximum force before complete failure.

In combination two, the V-SPR joint again fails due to failure of the joining part. In this case, however, the die-sided joining partner fails. Here, the greater maximum test force is again achieved by the slightly larger interlock. In addition, the longer rivet shank leads to a significant reduction of the minimum die-side material thickness. This reduces the load-bearing cross-section of the joint, which causes an increase of the stresses in the joint during testing. These stresses exceed the maximum tensile strength of the material, causing the material to crack and fail prematurely. The conventionally joined joint in combination 2 fails due to loosening of the rivet on the die side. During the test, the rivet tilts in the punch-sided sheet metal. However, the rivet does not unbutton from the joint. Before the joint is completely loosened, the punch-sided sheet is deformed causing great energy to be absorbed. Such failure is possible as the entire rivet head is formed into the punch-sided joining part. The increased contact surface between the rivet head and the punch-sided sheet prevents premature unbuttoning, which allows that some energy can still be absorbed even after the maximum force has been reached.

Combination 3 shows the greatest differences between SPR and V-SPR joints. The maximum force achieved is at a comparable level, but the V-SPR joints fail significantly earlier. The small interlock causes the rivet unbutton from the die-sided sheet. A plastic deformation of the parts to be joined cannot be detected. However, the simulation showed that a deeper penetration of the V-SPR rivet to increase the interlock is not possible due to the high stress concentration in the rivet shank. Further investigations should aim at changing the shank geometry to prevent premature collapse of the rivet when using high-strength materials on the die side. The formation of the joint can therefore be improved. The SPR joint has an interlock that is almost twice as large as the V-SPR joint, which enables the deformation of the punch-sided joint part and the associated increase in energy absorption. This is almost three times as high. The failure is comparable to combination 2.

Since a premature failure of the joint could be detected in two of three combinations, further objectives consist in taking suitable actions in order to positively influence this behaviour. As already mentioned, changing the rivet shaft or foot geometry could be one possibility. In addition, modifying the rivet head geometry could positively influence the energy absorption behaviour. It is intended to create a less rigid geometry, which also allows deformation under load and supports a later unbuttening of the rivet.

Figure 18 shows a compilation of exemplary test force–displacement curves of the SPR and the V-SPR process under cross tensile load as well as the evaluation of the absorbed energy. All combinations demonstrate an high level of strength. This refers to both the maximum force achieved and the displacement at failure. The scatter pattern of the cross tensile strength of the V-SPR joints is in all investigated joints slightly lower than that of the SPR joints.

The greatest differences can be seen in combination 3, which in turn can be attributed to the different degrees of interlock formation in the die-sided sheet. The V-SPR joint fails due to unbuttoning of the rivet. The cracks in the head area therefore do not negatively affect the load-bearing capacity. In the case of the SPR joint, the punch-sided aluminium sheet fails. The rivet remains in the die-sided

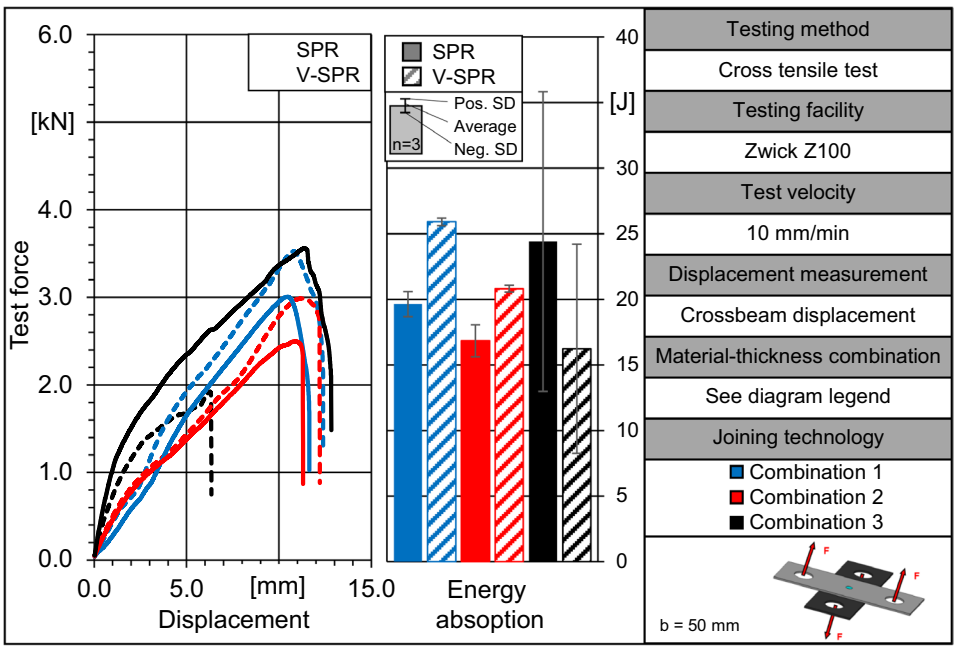

Fig. 18 Load bearing tests under cross tensile load; left: Exemplary test force-displacement curves for the SPR and V-SPR riveted joints for combinations 1–3, right: Comparison of the achieved energy absorption for the SPR and V-SPR riveted joints for combinations 1–3

joining partner. However, the results for both the SPR and the V-SPR joint show a large scatter. This can be attributed to the high-strength steel material on the punch side, which can lead to a fluctuating joint formation and thus different load-bearing capacities.

In combinations 1 and 2, the V-SPR joint exceeds the load-bearing capacity of the SPR process in each case. In both cases this is due to the higher interlock caused by the greater length of the multi-range capable rivet. The increased interlock results in both an increased maximum force and an increased energy absorption due to an later failure of the joints. Combination 1 results in the failure of the punch-sided joining part. The rivet remains locked in the die-sided joining partner. Damage to the rivet head formed by the forming process is not apparent. To illustrate the correlations, Fig. 19 shows exemplary fracture patterns of the three combinations under cross tensile load.

4 Conclusion

In the study presented here, the feasibility of the versatile semi-tubular self-piercing riveting process on joining multi-material structures was investigated. In this process, the rivet is initially set linearly, which is comparable to conventional joining processes. Subsequently, the rivet head is formed by means of enhanced punch-sided tool actuation, allowing the joining element to be adapted to the respective sheet thickness combination of the joint. The main conclusions are the following:

- Using the V-SPR process, three multi-material joints could be manufactured. Two of the chosen material-thickness combinations fulfilled the preferred joining directions for SPR processes, while the third did not.
- In all three joints, the joint formation was possible according to the specified quality-relevant parameters. In addition, the rivet could be adapted by forming the rivet head to different material thicknesses. An adjustment of the rivet length, as it would be necessary in conventional SPR-process was not required. Furthermore, the number of dies needed could be significantly reduced.
- Using a simulation model, head formation of the rivet was further investigated. In particular, the occurrence of high degrees of deformation leads to an increased stress concentration in the head area which leads to crack initiation.
- Cracking of the rivet head can occur when large changes in sheet thickness are to be covered or deep penetration of the rivet into the joined parts is not possible due to high-strength steels used on the die-side.
- In addition, the use of high-strength steel materials on the die side can due to the length of the rivet cause the rivet shank to bulge, which impairs the joint formation.
- The V-SPR joints demonstrate an excellent level of strength under shear- and cross tensile load which is comparable to the load-bearing behaviour of conventionally joined specimens.
- No negative influence on the load-bearing capacity under shear- and tensile load due to the formation of the rivet head could be detected. Premature failure of the joints as a result of failure of the auxiliary joining part is avoided.

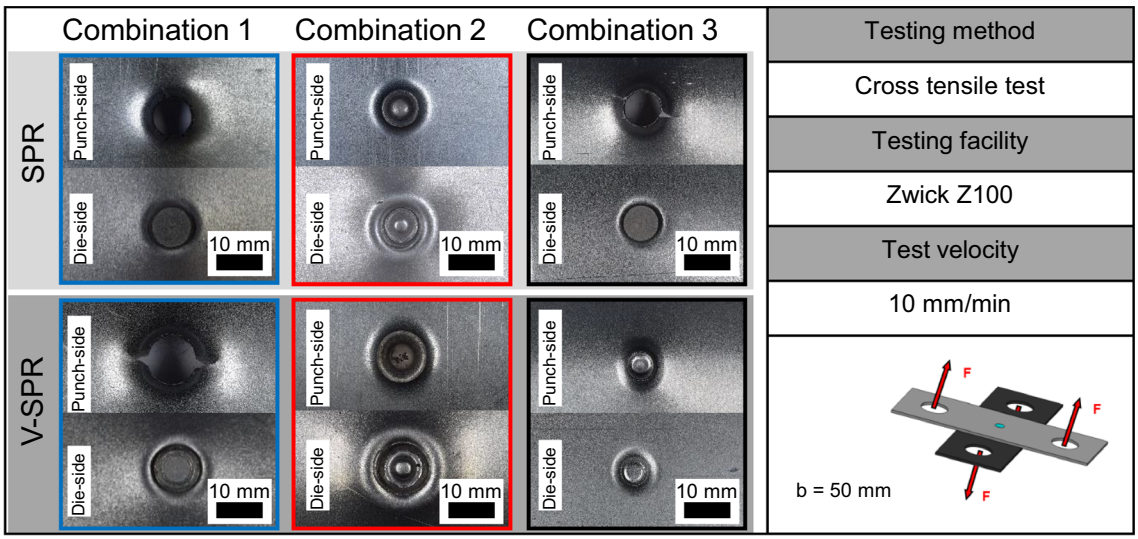

Fig. 19 Compilation of exemplary fracture patterns under cross tensile load for combination 1 to 3 (left: HCT590X t = 0.8 mm in EN AW-6014 T4 t = 2.0 mm [Combination 1]; centre: HCT590X t = 1.0 mm in EN AW-6014 T4 t = 1.5 mm [Combination 2]; right: EN AW-6014 T4 t = 1.5 mm in HCT590X t = 1.5 mm [Combination 3])

Acknowledgements Funded by the Deutsche Forschungsgemeinschaft (DFG, German Research Foundation)—TRR 285—Project-ID 418701707. The authors thank the German Research Foundation for their organisational and financial support. Furthermore, the authors would like to thank the company Lindemann und Söhne for providing the material which was needed for the production of the rivet prototypes.

Funding Open Access funding enabled and organized by Projekt DEAL.

References

1. Martinsen K, Hu SJ, Carlson BE (2015) Joining of dissimilar materials. CIRP Ann Manuf Technol 64:679–699. https://doi.org/10.1016/j.cirp.2015.05.006
2. DIN 8593-5 (2003) Fertigungsverfahren Fügen, Teil 5: Fügen durch Umformen Einordnung, Unterteilung, Begriffe
3. Voelkner W, Liebrecht F, Hahn O, Schulte A (1996) Untersuchungen zur optimierung des stanznietens mit halbhohlniet als universelles fügeverfahren zum verbinden von blechen und profilen. Europäische Forschungsgesellschaft für Blechverarbeitung e.V.
4. Hahn O, Klemens U (1996) Fügen durch Umformen, Nieten und Durchsetzfügen - Innovative Verbindungsverfahren für die Praxis: Dokumentation 707. Studiengesellschaft Stahlanwendung e.V.
5. Meschut G, Merklein M, Brosius A et al (2022) Review on mechanical joining by plastic deformation. J Adv Join Process 5:100113. https://doi.org/10.1016/j.jajp.2022.100113
6. Trinick RJ (2015) Method for forming a joint using a self-piercing rivet
7. Uhe B, Kuball C-M, Merklein M, Meschut G (2020) Improvement of a rivet geometry for the self-piercing riveting of high-strength steel and multi-material joints. Prod Eng 14:417–423. https://doi.org/10.1007/s11740-020-00973-w
8. Li Y, Wei Z, Li Y, et al (2013) Friction Self-Piercing Riveting (F-SPR) of AA6061-T6 to AZ31B. In: Volume 2B: Advanced Manufacturing. American Society of Mechanical Engineers, pp 1–7
9. Alves LM, Afonso RM, Martins PAF (2020) Double-sided self-pierce riveting. Int J Adv Manuf Technol 108:1541–1549. https://doi.org/10.1007/s00170-020-05503-7
10. Neugebauer R, Jesche F, Israel M (2010) Enlargement of the application range of solid punch riveting by two-piece dies. Int J Mater Form 3:999–1002. https://doi.org/10.1007/s12289-010-0938-2
11. Kappe F, Wituschek S, Bobbert M, Meschut G (2022) Determining the properties of multi-range semi-tubular self-piercing riveted joints. Prod Eng 16:363–378. https://doi.org/10.1007/s11740-022-01105-2
12. Novelis Global Automotive (2019) Datasheet: Novelis Advanz™ 6F - e170; Aluminium Sheet For Exterior Applications
13. Salzgitter Flachstahl GmbH (2017) Datasheet: HCT590X+Z (HCT600XD / HC340XD*/ CR330Y590T-DP**); Mehrphasenstähle zum Kaltumformen - Dualphasenstähle
14. Böhnke M, Kappe F, Bobbert M, Meschut G (2021) Influence of various procedures for the determination of flow curves on the predictive accuracy of numerical simulations for mechanical joining processes. Mater Test 63:493–500. https://doi.org/10.1515/mt-2020-0082
15. DVS/EFB-Merkblatt 3480–1 (2010) Testing of Properties of Joints Testing of Properties of mechanical and hybrid (mechanical/bonded) joints—Stiffness analysis of mechanical joints
16. Kappe F, Bobbert M, Meschut G (2021) New approach for versatile self piercing riveting: joining system and auxiliary part. Key Eng Mater 883:3–10. https://doi.org/10.4028/www.scientific.net/KEM.883.3
17. Kappe F, Schadow L, Bobbert M, Meschut G (2022) Increasing flexibility of self-piercing riveting by reducing tool–geometry combinations using cluster analysis in the application of multi-material design. Proc Inst Mech Eng Part L J Mater Des Appl 146442072110709. https://doi.org/10.1177/14644207211070992